HOKKAIDO UNIVERSITY

Title	Crystal structures of synthetic 7 Å and 10 Å manganates substituted by mono- and divalent cations
Author(s)	Kuma, Kenshi; Usui, Akira; Paplawsky, William et al.
Citation	Mineralogical magazine, 58(392), 425-447 https://doi.org/10.1180/minmag.1994.058.392.08
Issue Date	1994-09
Doc URL	https://hdl.handle.net/2115/53250
Type	journal article
File Information	58-392-425.pdf

Hokkaido University Collection of Scholarly and Academic Papers : HUSCAP

Crystal structures of synthetic 7 Å and 10 Å manganates substituted by mono- and divalent cations

KENSHI KUMA

Department of Chemistry, Faculty of Fisheries, Hokkaido University, 3-1-1 Minato-cho, Hakodate, Hokkaido 041, Japan

AKIRA USUI

Marine Geology Department, Geological Survey of Japan, 1-1-3 Higashi, Tsukuba, Ibaraki 305, Japan

AND

WILLIAM PAPLAWSKY, BENJAMIN GEDULIN AND GUSTAF ARRHENIUS

Scripps Institution of Oceanography, University of California at San Diego, La Jolla, CA 92093, USA

Abstract

The crystal structures of synthetic 7 Å and 10 Å manganates, synthetic birnessite and buserite, substituted by mono- and divalent cations were investigated by X-ray and electron diffractions. The monoclinic unit cell parameters of the subcell of lithium 7 Å manganate, which is one of the best ordered manganates, were obtained by computing the X-ray powder diffraction data: a = 5.152 Å, b = 2.845 Å, c = 7.196 Å, β = 103.08°. On the basis of the indices obtained by computing the X-ray diffraction data of Li 7 Å manganate, monovalent Na, K and Cs and divalent Be, Sr and Ba 7 Å manganates were interpreted as the same monoclinic structure with β = 100–103° as that of Li 7 Å manganate, from their X-ray diffraction data. In addition, divalent Mg, Ca and Ni 10 Å manganates were also interpreted as the same monoclinic crystal system with β = 90–94°. The unit cell parameters, especially a, c and β, change possibly with the type of substituent cation probably because of the different ionic radius, hydration energy and molar ratio of substituent cation to manganese. However, these diffraction data, except for those of Sr and Ba 7 Å and Ca and Ni 10 Å manganates, reveal only some parts of the host manganese structure with the edge-shared [MnO_6] octahedral layer. On the other hand, one of the superlattice reflections observed in the electron diffractions was found in the X-ray diffraction lines for heavier divalent cations Sr and Ba 7 Å and Ca and Ni 10 Å manganates. The reflection presumably results from the substituent cation position in the interlayer which is associated with the vacancies in the edge-shared [MnO_6] layer and indicates that the essential vacancies are linearly arranged parallel to the b-axis. Furthermore, the characteristic superlattice reflection patterns for several cations, Li, Mg, Ca, Sr, Ba and Ni, manganates were interpreted that the substituent cations are regularly distributed in the interlayer according to the exchange percentage of substituent cation to Na^+. In contrast, the streaking in the a-direction observed strongly in the electron diffractions for heavier monovalent cations, K and Cs, manganates probably results from the disordering of their cations in the a-direction in the interlayer.

KEYWORDS: 7 Å manganate, 10 Å manganate, X-ray diffraction, electron diffraction, crystal structure.

Introduction

IN several studies the marine 7 Å and 10 Å manganates in manganese nodules and crusts are concluded as being structurally identical or similar to synthetic 7 Å and 10 Å manganates and terrestrial minerals such as birnessite, buserite

Mineralogical Magazine, September 1994, Vol. 58, pp. 425–447
© Copyright the Mineralogical Society

and todorokite (Buser and Grütter, 1956; Arrhenius *et al.*, 1979; Giovanoli and Brütsch, 1979; Giovanoli, 1980; Hariya, 1980; Arrhenius and Tsai, 1981; Crane, 1981; Mellin, 1981). The synthetic 7 Å and 10 Å manganates offer simple analogues of the phyllomanganate minerals birnessite and buserite, which appear to typify the hydrothermal manganese oxides deposited along submarine oceanic spreading centers (Moore and Vogt, 1976; Corliss *et al.*, 1978) and island arcs (Cronan *et al.*, 1982; Usui *et al.*, 1989; Usui and Nishimura, 1992). This mineralogy differs from the todorokite–vernadite of marine manganese nodules of low-temperature, hydrogenous origin (Burns and Burns, 1977, 1978; Turner *et al.*, 1982). However, the crystal structures of synthetic 7 and 10 Å manganates as well as marine manganates are still incompletely known because of their small crystallite sizes, precluding single crystal analysis by X-ray diffraction, structural transformation and analysis. The most common crystalline manganese phases identified in manganese nodules and crusts by X-ray powder diffraction patterns are expandable and fixed 10 Å manganates, buserite and todorokite, which were characterized by X-ray diffraction lines at 9.6–9.7, 4.80–4.85, 2.40–2.45 and 1.40–1.42 Å, and 7 Å manganate, birnessite, at 7.0–7.3 and 3.5–3.6 Å as well as others around 2.40–2.45 and 1.40–1.42 Å (Glasby, 1972; Giovanoli and Bürki, 1975; Burns and Burns, 1977, 1979, 1981; Usui *et al.*, 1978, 1989). Such lines occur in X-ray diffraction patterns of synthetic 7 Å and 10 Å manganates reported in derivatives of a synthetic sodium manganese oxide hydrate, Na 7 Å and 10 Å manganates (Feitknecht and Marti, 1945; Wadsley, 1950*a*, *b*; McKenzie, 1971; Giovanoli, 1980).

Na 10 Å manganate with cation exchange properties is synthesized by oxidation of freshly precipitated $Mn(OH)_2$ suspension in cold aqueous NaOH with flowing O_2 gas (Wadsley, 1950*a*, *b*; Giovanoli *et al.*, 1970*a*, 1975; Crane, 1981). In air at room temperature, the synthetic Na 10 Å manganate dehydrates readily to Na 7 Å manganate, resulting in contraction from 10 Å to 7 Å basal spacing. The cation exchange in Na 10 Å manganate by divalent cations with high hydration energy, such as Cu, Ni, Co, Ca and Mg, stabilize the 10 Å spacing against contraction to 7 Å with decreasing strength Cu ≫ Ni > Zn ≫ Ca > Mg (Giovanoli *et al.*, 1975; Giovanoli and Brütsch, 1979; Usui, 1979; Crane 1981). The synthetic Na manganate consists of elongated platelets which give an electron diffraction pattern with pseudohexagonal symmetry and weak superlattice reflections (Giovanoli *et al.*, 1970*a*). In the structure of synthetic Na 7 Å manganate, $Na_4Mn_{14}O_{27}\cdot 9H_2O$, proposed by Giovanoli *et al.* (1970*a*), one out of every six $[MnO_6]$ octahedra is vacant, and Mn^{2+} and/or Mn^{3+} are considered to lie above and below these vacancies in the edge-shared $[MnO_6]$ octahedral layer. The positions of the Na^+ ions in the intermediate layer are uncertain. The X-ray and electron diffraction measurements (Giovanoli *et al.*, 1970*a*, *b*) proposed that synthetic Na 7 Å manganate is a double layer manganate (IV) structure resembling other manganates such as chalcophanite ($Zn_2Mn_6O_{14}\cdot 6H_2O$) and that the orthorhombic unit cell parameters are a = 8.54 Å, b = 15.39 Å and c = 14.26 Å. However, Post and Veblen (1990) determined the crystal structures of the subcells of synthetic Na, Mg and K 7 Å manganates by the Rietveld method and electron diffraction. The subcells have the monoclinic unit cell parameters: Na: a = 5.175 Å, b = 2.850 Å, c = 7.337 Å, β = 103.18°; Mg: a = 5.049 Å, b = 2.845 Å, c = 7.051 Å, β = 96.65°; K: a = 5.149 Å, b = 2.843 Å, c = 7.176 Å, β = 100.76°. Only the b parameter is relatively constant for all three phases at 2.84–2.85 Å, which is the intralayer Mn–Mn distance. The wide range of unit cell parameters are evidence of the flexibility of the structural framework. The sheets of water molecules and hydroxyl groups are located between layers of edge-shared $[MnO_6]$ octahedra. Synthetic 10 Å manganate is considered to have a similar layered structure, but additional OH^- ions and H_2O molecules are present so that the vacancy-ordered layers of $[MnO_6]$ octahedra are 9.6–10.1 Å apart (Giovanoli, 1980).

The fact that the manganate crystal size does not exceed the order of 1 μm excludes the possibility of complete solution of the crystal structure by X-ray diffraction analysis, which requires single crystals at least a hundred times larger. Excellent single exposures are obtained by selected area electron diffraction analysis, but dynamic diffraction effects preclude quantitative interpretation of the interactions of the diffracted beams. However, it is possible to decide the unit cell parameters of the various manganate structures and the precise location of the exchangeable interlayer cations by combination of the symmetry information from single crystal electron diffraction and cell dimension data obtainable from X-ray powder diffraction. In this study, the unit cell parameters of synthetic 7 Å and 10 Å manganates substituted by various cations were determined from their diffraction data. In addition, their characteristic electron diffraction patterns were interpreted from a point of view for the substituent cations.

Materials and methods

Synthetic manganate samples. Na 10 Å manganate as a host material was synthesized by oxidation of freshly precipitated $Mn(OH)_2$ in alkaline suspension, supersaturated with oxygen, at low temperature for 1 day (Wadsley, 1950*a*, *b*; Giovanoli *et al.*, 1970*a*, 1975; Crane, 1981). 1000 ml of 0.5 M $MnCl_2$ solution cooled to 0°C were added to 1250 ml of 5 M NaOH solution cooled to 0°C on an iced bath and stirred with a Teflon-coated magnetic stirrer, followed by bubbling molecular oxygen at a flow rate of 25 ml/min for 1 day. The degree of oxidation of the divalent Mn ions determines the product and crystal size formed, resulting in the formation of thin two dimensional δ-MnO_2 (Buser and Graf, 1955*a*, *b*) and/or small crystalline Na 10 Å manganate at higher oxygen flow rate. The precipitate was filtered through a 0.45 μm Millipore filter and washed with distilled water until the pH of the filtrate had decreased to the range 9.5–10.0. To ensure full hydration, keeping the 10 Å structure stable, the product was stored as aqueous alkaline suspension, from which aliquots were removed as needed for the various investigations.

The cation substitution was carried out by shaking 1 g of the synthetic Na 10 Å manganate into 50 ml of each 0.5 M solution of monovalent (Li, K and Cs chlorides) and divalent (Be, Mg, Ca, Sr, Ba and Ni chlorides) cations. The cation exchange reaction time was 3 days. Each synthetic manganate substituted with cations was filtered through a 0.45 μm filter, rinsed repeatedly with distilled water and dried in air at room temperature for at least 3 days.

Analyses of manganese and substituent cations. The contents of manganese and substituent cations, except for Cs and Be, in the synthetic manganates were analyzed by an atomic absorption spectrophotometer (AA) after digestion of each sample (25 mg) suspended into 100 ml of distilled water with 20 ml of concentrated HCl and then suitable dilution. The molar ratio of substituent cation to manganese in each manganate was consequently determined.

X-ray powder diffraction analysis. The crystal structures of manganates substituted by various cations, in addition of Na 7 Å manganate as a host material, were studied by X-ray powder diffraction, which was carried out on air-dried manganates to establish the rank of contraction of the basal *c*-spacing, *d* (001), to obtain three dimensional information and to determine the unit cell parameters of the different manganate structures by combination with two dimensional information (*a*-*b* plane) from electron diffraction. All air-dried manganates were allowed to equilibrate at ambient laboratory conditions for at least 3 days. General Electric XRD-5 diffractometers modified for automated input and data processing were used with a step size of 0.02° and count time of 0.5 sec at 2θ range from 6° to 70°; radiation employed was filtered Cu-$K\alpha$ (40 kV, 20 mA) and measured with a Philips scintillation counter.

Electron diffraction and transmission electron microscopy image. A small amount of each synthetic manganate from well dispersed aqueous suspensions was placed on carbon coated formvar film microscope grids. The image and electron diffraction of the single crystal was observed by a transmission electron microscope, Hitachi H500 instrument, at accelerating voltage of 100 kV. The directions in the diffraction pattern were determined by superimposing the image of the long edge of a molybdenum trioxide (MoO_3) crystal in order to obtain the correlation of directions in the image and the diffraction pattern (Beeston *et al.*, 1972). In addition, the accurate value of camera length was determined from the unit cell parameter of gold in the electron diffraction pattern.

Results and discussion

The manganates substituted by alkali, Li, Na, K and Cs, and alkali earth, Be, Sr and Ba, cations collapsed to 7 Å spacing at ambient atmospheric water vapour pressure (Table 1). In contrast, Mg, Ca and Ni manganates retained the 10 Å basal spacing with the weakly coordinated water molecules in the interlayer under air dried condition probably because of the higher hydration energy of Mg^{2+}, Ca^{2+} and Ni^{2+} (Table 1). In fact, X-ray diffraction of Mg and Ca manganates dehydrated by heating at 60 and 50°C, respectively, for 3 hr confirmed the transition to 7 Å spacing (Table 1) resulting from the loss of coordinated water (8–9 mass %) in the interlayer measured by a thermogravimetric analysis. Tejedor-Tejedor and Paterson (1978) emphasized the effect of relative humidity on the stability and lattice dimensions of the synthetic 10 Å manganates substituted by alkali and alkali earth cations. They reported that all the monovalent cation derivatives, including unsubstituted Na manganate, collapsed immediately to 7 Å spacing, while Mg and Ca manganates imparted the most stability of 10 Å spacing. It has been reported that transition metal divalent cations such as Co, Ni, Cu and Zn, which are more tightly built into the structure of 10 Å manganate, stabilize 10 Å spacing (Giovanoli *et al.*, 1975; Usui, 1979; Giovanoli, 1980; Crane, 1981). Although Be^{2+}

TABLE 1. Ionic radii and hydration energy of substituent cations, composition of the synthetic manganates analysed by AA and basal *c*-spacing of the manganates observed in X-ray powder diffraction patterns

Substituent cation (charge)	Ionic radius Å 1)	Hydration energy -kcal/mol 2)	Me/Mn molar ratio	Mn wt.%	Me wt.%	Exchange percentage % 3)	*c*-spacing *d*(001) Å 4)
(+1)							
Li	0.68	122	0.345	45.7	1.99	89	7.006
Na	0.97	98	0.388	44.4	7.21	100	7.128
Na* 5)							10.140
K	1.33	81	0.296	45.0	9.47	76	7.032
Cs	1.67	68	–	43.2	–	–	7.268
(+2)							
Be	0.35	591	–	49.5	–	–	7.200
Mg	0.66	456	0.161	49.3	3.52	83	9.606
Mg* 6)							6.834
Ca	0.99	381	0.111	45.3	3.65	57	9.984
Ca* 6)							7.012
Sr	1.12	346	0.098	48.1	7.51	51	7.008
Ba	1.34	315	0.071	49.3	8.77	37	7.042
Ni	0.69	594	0.168	44.0	7.92	87	9.654

1): Ahrens ionic radii (CN = VI) (Ahrens, 1952; Shannon and Prewitt, 1969).
2): Hydration energy (Rosseinsky, 1965)
3): Exchange percentage of substituent cation to Na^+ on the basis of the molar ratio of Na/Mn for Na manganate.
4): Basal *c*-spacings calculated from 2 × *d*(002) and 3 × *d*(003) in the X-ray diffraction data for 7 Å and 10 Å manganates, respectively (Table 2, 3 and 4).
5): Basal *c*-spacing for Na 10 Å manganate (moist sample without drying).
6): Basal *c*-spacings for Mg and Ca 7 Å manganates (samples dried at 60 and 50°C, respectively, for 1 day).
–: not determined

has the highest hydration energy in this study, Be manganate collapsed to 7 Å spacing under air dried condition probably because of the smallest ionic radius (Table 1). These results suggest that the strength of the water complex rather than the size of cations primarily determines the interplanar spacing and the stability of 10 Å manganate structure. The infrared spectra of 10 Å and 7 Å manganates (Potter and Rossman, 1979) indicated that synthetic 10 Å and 7 Å manganates have analogous structures, the contraction from 10 Å to 7 Å basal plane spacing in X-ray diffraction patterns being the result of water loss alone rather than a structural rearrangement of $[MnO_6]$ octahedral framework.

Unit cell parameters of synthetic 7 Å and 10 Å manganates. It is possible to derive the unit cell parameters of synthetic 7 Å and 10 Å manganates structure by combination of information from the cell dimension data from X-ray powder diffraction and single crystal electron diffraction.

Basal plane reflection (00*l*) as well as general reflections (*hkl*) in turn can be measured by X-ray powder diffraction as shown in Figs. 1 and 2. The electron microscope image of typical 7 Å manganates shows the single crystals which have rectangular shape with crystal size of 1–2 μm as shown in Fig. 3*a*. These crystals are characteristically lath-shaped and thin sheets and are preferably oriented with *c*-axis, the expandable lattice dimension parallel to the electron beam, and normal to the *a*–*b* plane. Therefore, the information on the *a*–*b* plane {(*h*00), (*hk*0) and (0*k*0)} can be obtained by electron diffraction (Figs. 3 and 4). It should be noted that electron microscopy studies of synthetic 10 Å manganates

(a) Li 7 Å manganate

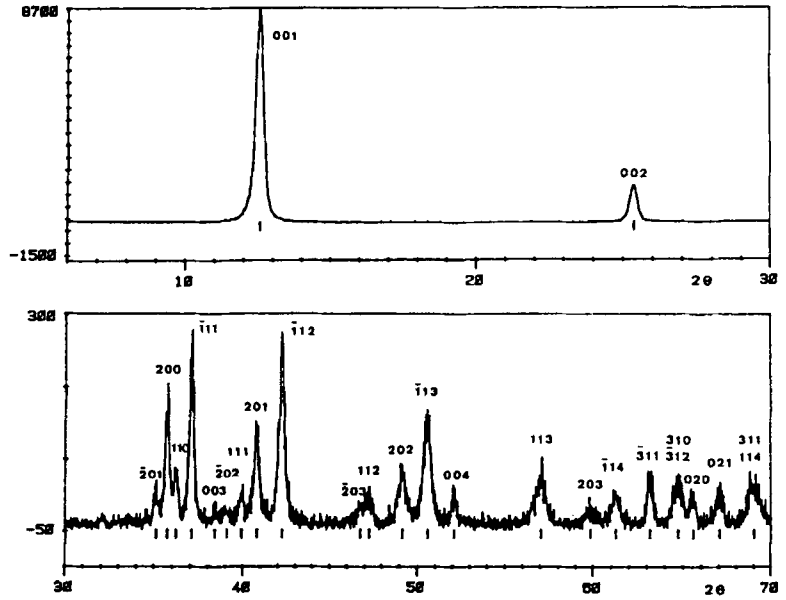

(b) Ba 7 Å manganate

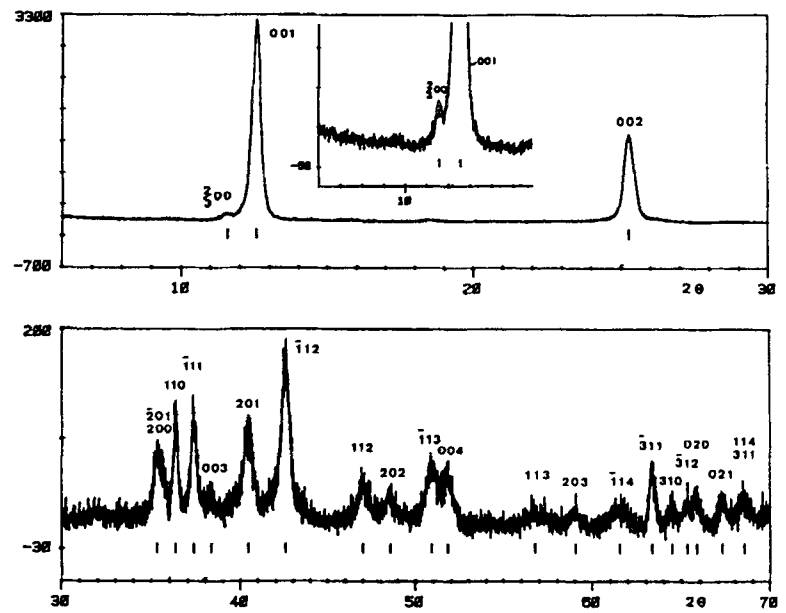

FIG. 1. X-ray powder diffractogram of synthetic 7 Å manganates: (*a*) Li 7 Å manganate; (*b*) Ba 7 Å manganate. The indices for Li 7 Å manganate were obtained by computing the *d*-values in the X-ray diffraction data (Table 2). Those for Ba 7 Å manganates were obtained by hand calculation as a monoclinic crystal system on the basis of the indexed results for Li 7 Å manganate (Table 3*f*).

(a) Ca 10 Å manganate

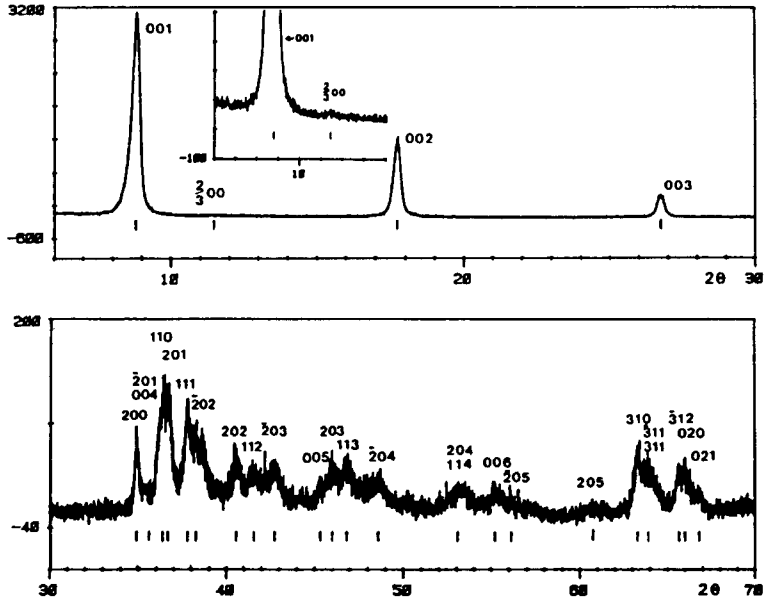

(b) Ni 10 Å manganate

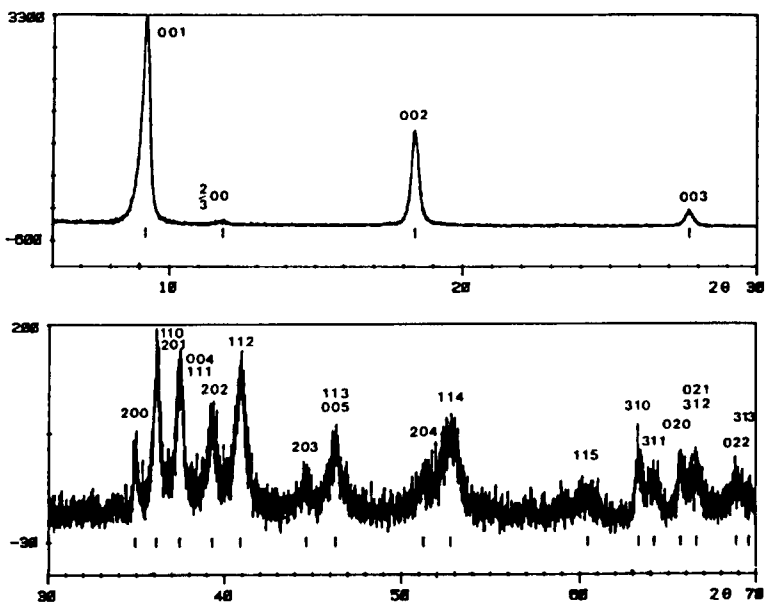

FIG. 2. X-ray powder diffractograms of synthetic 10 Å manganates: (*a*) Ca 10 Å manganate; (*b*) Ni 10 Å manganate. The indices were obtained by hand calculation as a monoclinic crystal system on the basis of the indexed results for Li 7 Å manganate (Table 4*b* and *c*).

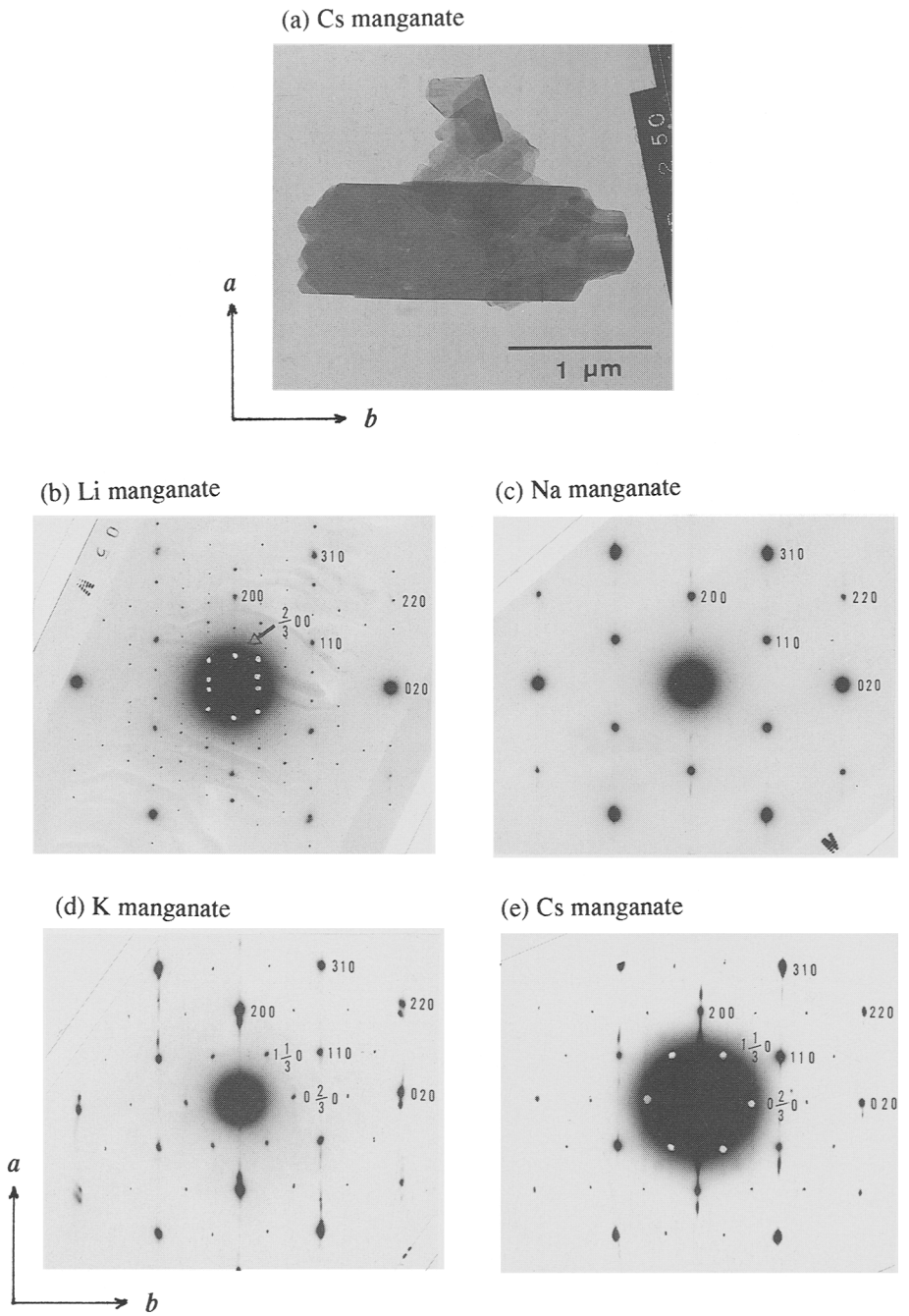

FIG. 3. Electron micrograph and electron diffraction patterns in the *a-b* plane of synthetic monovalent cation manganates: (*a*) electron micrograph of typical manganate (Cs manganate); (*b*) Li manganate; (*c*) Na manganate; (*d*) K manganate; (*e*) Cs manganate. The reflection marked with arrow: (⅔ 0 0). The indices were obtained as an orthorhombic crystal system in the *a-b* plane on the basis of fundamental pseudohexagonal reflections.

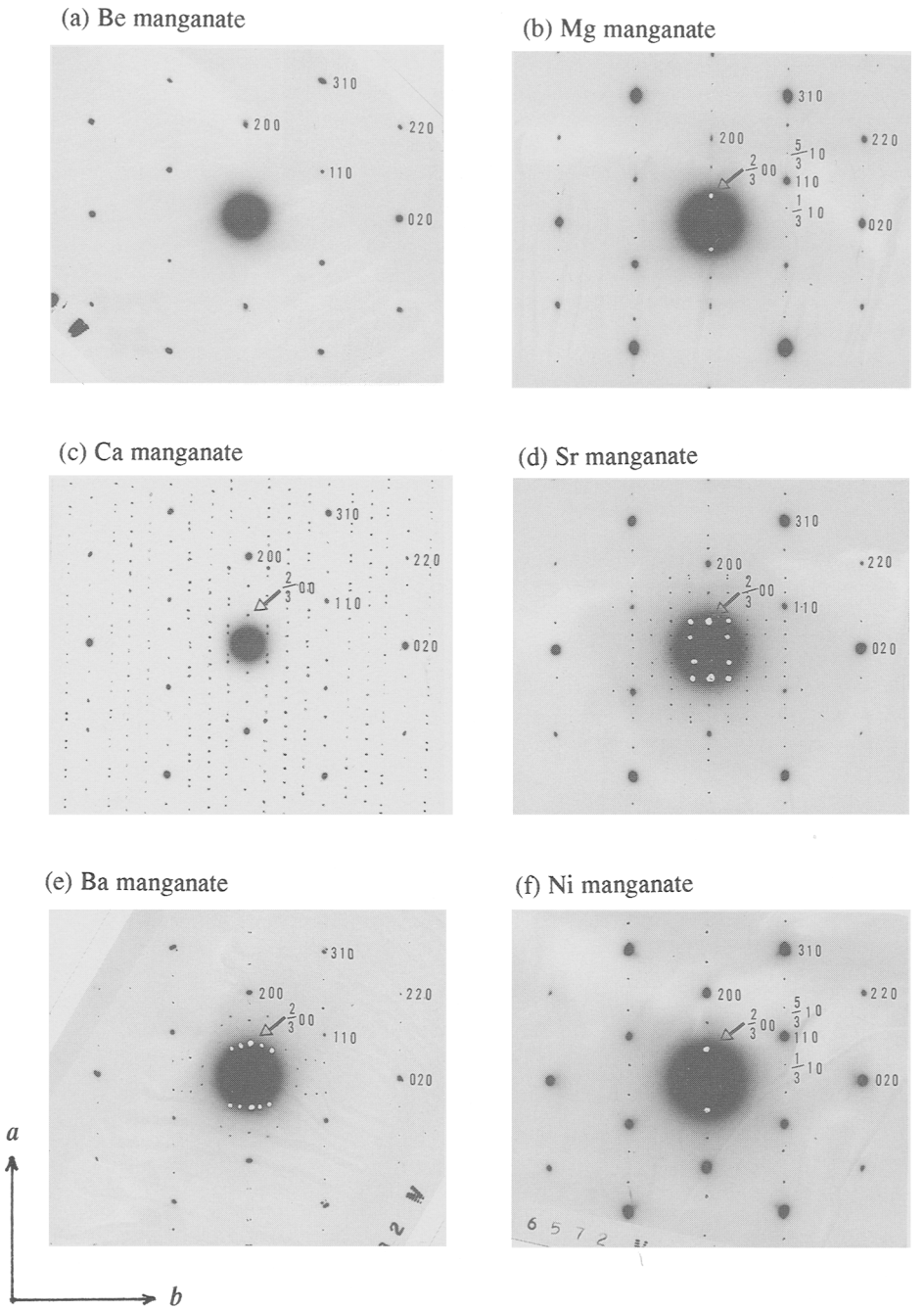

FIG. 4. Electron diffraction patterns in the *a-b* plane of synthetic divalent cation manganates: (*a*) Be manganate; (*b*) Mg manganate; (*c*) Ca manganate; (*d*) Sr manganate; (*e*) Ba manganate; (*f*) Ni manganate. The reflection marked with arrow: (⅔ 0 0). The indices were obtained as an orthorhombic crystal system in the *a-b* plane on the basis of fundamental pseudohexagonal reflections.

TABLE 2. Indexed interplanar spacings of Li 7 Å manganate obtained by computing the X-ray diffraction data. ($a=5.152$ Å, $b=2.845$ Å, $c=7.196$ Å, $\beta=103.08°$)

Line No.	Intensity I/I_o (×100)	$d_{(meas.)}$ Å	$d_{(calc.)}$ Å	hkl	$d_{(meas.)}-d_{(calc.)}$ (×1000)
1	100	7.016	7.009	001	7
2	17	3.503	3.505	002	–2
3	1	2.553	2.553	$\bar{2}01$	0
4	2	2.509	2.509	200	0
5	1	2.475	2.475	110	0
6	3	2.420	2.420	$\bar{1}11$	0
7	<1	2.336	2.336	003	0
8	<1	2.299	2.302	$\bar{2}02$	–3
9	<1	2.256	2.256	111	0
10	2	2.209	2.209	201	0
11	3	2.136	2.137	$\bar{1}12$	–1
12	<1	1.941	1.943	$\bar{2}03$	–2
13	<1	1.923	1.923	112	0
14	1	1.850	1.851	202	–1
15	2	1.802	1.802	$\bar{1}13$	0
16	1	1.751	1.752	004	–1
17	1	1.612	1.611	113	1
18	<1	1.543	1.544	203	–1
19	<1	1.511	1.512	$\bar{1}14$	–1
20	1	1.470	1.470	$\bar{3}11$	0
21	1	1.438	1.442	310	–4
			1.436	$\bar{3}12$	2
22	<1	1.422	1.422	020	0
23	<1	1.394	1.394	021	0
24	1	1.361	1.361	311	0
			1.360	114	1

$d_{(meas.)}$ and $d_{(calc.)}$ were d-spacings measured from X-ray diffraction pattern (Fig. 1) and calculated by computing the X-ray diffraction data, respectively.

result in a transformation from an initial 10 Å basal spacing to 7 Å due to the exposure of the samples to high vacuum in the electron microscope.

These electron diffraction patterns contain the fundamental and imperfect hexagonal reflections. Only first order reflections appear for Be 7 Å manganate (Fig. 4*a*), while those for the other cation manganates show superlattice reflections in the *a*–*b* plane (Li, K, Cs, Mg, Ca, Sr, Ba and Ni manganates; Figs. 3 and 4) and/or streaking in the *a*-direction (Na, K and Cs manganates; Fig. 3). Only observation of fundamental hexagonal reflections for Be manganate may be because of lower scattering power of light element Be and/or lower exchange percentage of Be to Na^+. The fundamental hexagonal reflections for all the cation manganates were temporarily interpreted as an isotropic manganate layer structure based on edge-shared [MnO_6] octahedra. The morphology and electron diffraction data indicate that the observed hexagonal symmetry is a pseudosymmetry; the true unit cell appears to be actually orthorhombic or monoclinic. All the cation manganates displayed strong reflections, (200), (020), (110), (310), etc. in Figs. 3 and 4. These fundamental lattice reflections presumably appear as a result of the ordered edge-shared [MnO_6] octahedra extending in the *a*–*b* plane.

In this study, the Li 7 Å manganate structure is one of the best ordered manganates in X-ray diffraction (Fig. 1*a*). The diffraction data of Li 7 Å manganate was therefore selected to find the unit cell from the X-ray powder diffraction pattern by computing the diffraction data in the programme of which principles were described by Visser (1969). The indexed result (Table 2 and Fig. 1*a*) indicates that the Miller indices can be expressed as a monoclinc crystal system by only combination between basal spacing, (00*l*), observed in X-ray

TABLE 3. Indexed interplanar spacings of Na, K, Cs, Be, Sr and Ba 7 Å managantes observed in X-ray diffraction lines on the basis of the indexed results for Li 7 Å manganate. The star marked lines (*) were chosen in order to match the indices of all lines as a monoclinic crystal system.

(a) Na 7 Å manganate (a=5.164 Å, b=2.848 Å, c=7.314 Å, β=102.96°)

Line No.	Intensity I/I_o (×100)	$d_{(meas.)}$ Å	$d_{(calc.)}$ Å	*hkl*	$d_{(meas.)}-d_{(calc.)}$ (×1000)
1	100	7.133	7.128	001	5
* 2	25	3.564	3.564	002	0
3	<1	2.560	2.560	$\bar{2}01$	0
* 4	3	2.516	2.516	200	0
5	1	2.482	2.479	110	3
6	3	2.426	2.426	$\bar{1}11$	0
7	<1	2.375	2.376	003	–1
8	<1	2.321	2.315	$\bar{2}02$	6
9	<1	2.258	2.265	111	–7
10	1	2.219	2.221	201	–2
11	2	2.150	2.149	$\bar{1}12$	1
12	<1	1.935	1.937	112	–2
13	1	1.863	1.868	202	–5
14	1	1.821	1.818	$\bar{1}13$	4
15	1	1.783	1.782	004	1
16	<1	1.632	1.628	113	4
17	<1	1.557	1.561	203	–4
18	<1	1.532	1.529	$\bar{1}14$	4
*19	1	1.473	1.473	$\bar{3}11$	0
20	1	1.444	1.445	310	–1
			1.440	$\bar{3}12$	4
*21	1	1.424	1.424	020	0
22	1	1.395	1.396	021	–1
23	<1	1.380	1.377	114	3
24	<1	1.364	1.366	311	–2

diffraction and fundamental pseudohexagonal reflections, (200), (020), (110) and (310), in electron diffraction and are in remarkable agreement with our above assumption. Host manganese structure of Li 7 Å manganate is monoclinic with unit cell parameters, a = 5.152 Å, b = 2.845 Å, c = 7.196 Å and β = 103.08° (Fig. 5).

On the basis of the indexed results for Li 7 Å manganate, the unit cell parameters of other 7 Å and 10 Å manganates were determined from their X-ray diffraction data by hand calculation as a monoclinic crystal system since the d-values of weak lines in X-ray diffraction data possibly caused the computed error. Finally, the star marked lines (*) as shown in Tables 3 and 4 were chosen in order to match the indices of all diffraction lines and calculate the unit cell parameters as a monoclinic crystal system. Consequently, the differences between measured and calculated d-values of the diffraction lines, especially for Na, K and Ba 7 Å manganates (Table 3*a*, *b* and *f*, respectively), are appreciably smaller and all lines are regularly indexed. These parameters, especially a, c and β, change possibly by the type of substituent cation, while b is relatively constant, 2.844–2.848 Å for monovalent and 2.828–2.849 Å for divalent cations (Table 5) which is the intralayer Mn–Mn layer. These indices remarkably coincided with those obtained by computing for Li 7 Å manganate and indicated the monoclinic structure with β = 100–103° and 90–94° for 7 Å manganates and stable Mg, Ca and Ni 10 Å manganates, respectively. Moreover, the angle β determined from X-ray diffraction data (data not shown) of Na 10 Å manganate (moist sample without drying) was 99.22° similar to that, 102.96°, in Na 7Å manganate (Table 5). The angle β in Mg 7 Å manganate (sample dried at 60°C for

TABLE 3. (*contd.*)

(*b*) K 7 Å manganate ($a = 5.156$ Å, $b = 2.846$ Å, $c = 7.146$ Å, $\beta = 100.23°$)

Line No.	Intensity I/I_o (×100)	$d_{(meas.)}$ Å	$d_{(calc.)}$ Å	*hkl*	$d_{(meas.)}-d_{(calc.)}$ (×1000)
1	100	7.041	7.032	001	9
*2	21	3.516	3.516	002	0
*3	1	2.537	2.537	200	0
			2.534	$\bar{2}01$	3
4	1	2.479	2.482	110	–3
5	2	2.408	2.407	$\bar{1}11$	1
6	<1	2.344	2.344	003	0
7	2	2.257	2.262	201	–5
			2.256	$\bar{2}02$	1
8	2	2.118	2.116	$\bar{1}12$	2
9	<1	1.943	1.950	112	–7
10	1	1.901	1.903	202	–2
			1.897	$\bar{2}03$	4
11	1	1.787	1.783	$\bar{1}13$	4
12	1	1.759	1.758	004	1
13	<1	1.631	1.635	113	–4
14	<1	1.583	1.587	203	–4
15	<1	1.500	1.497	$\bar{1}14$	3
*16	1	1.469	1.469	$\bar{3}11$	0
17	<1	1.454	1.455	310	–1
*18	1	1.423	1.423	020	0
			1.422	$\bar{3}12$	1
19	<1	1.393	1.395	021	–2
20	<1	1.383	1.383	311	0
21	<1	1.377	1.389	114	–2

1 day) was 95.26°, also similar to that, 93.97°, in air-dried Mg 10 Å manganate (Table 5). These results probably suggest that a little increase of angle β by contraction from 10 Å to 7 Å spacing is accomplished with the parallel transformation of the *a–b* plane along the perpendicular axis to the *a–b* plane by the loss of coordinated water in the interlayer. The wide range of unit cell parameters are evidence of the flexibility of the structural framework. They are also expressed by only combination between basal spacing, (00*l*), observed in all X-ray diffractions (Tables 2, 3 and 4) and fundamental pseudohexagonal reflections, (200), (020), (110) and (310), observed in all electron diffractions (Figs. 3 and 4), although superlattice reflections in the *a–b* plane and/or streaking in the *a*-direction were observed in their electron diffractions, except for Be 7 Å manganate. These results suggest that the X-ray diffraction data, except for those of Sr and Ba 7 Å and Ca and Ni 10 Å manganates, reveal only fundamental monoclinic structure of the edge-shared $[MnO_6]$ octahedral layer. Recently, Post and Veblen (1990) determined the crystal structures of the subcells of synthetic Na, Mg and K 7 Å manganates by the Rietveld method and electron diffraction. The subcells have monoclinic unit cell parameters (Table 5), remarkably consistent with those determined in this study. The angle β ranges from over 103° in Na 7 Å manganate to 96.65° in Mg 7 Å manganate. Only the *b* parameter is relatively constant for all three phases at 2.84–2.85 Å. However, X-ray diffraction lines of the heavier divalent cations Sr and Ba 7 Å and Ca and Ni 10 Å manganates (Table 3*e*, *f* and Fig. 1*b*, Table 4*b* and Fig. 2*a*, and Table 4*c* and Fig. 2*b*, respectively) includes a weak line which was related to a superlattice reflection (⅔ 0 0), with a periodicity of three between fundamental reflection (200), observed in the electron diffractions of Li, Mg, Ca, Sr, Ba and Ni manganates (Fig. 3*b*, 4*b*, *c*, *d*, *e* and *f*, respectively). Therefore, in order to reveal a detailed host manganate structure, it is expected to interpret the substituent

TABLE 3. (*contd.*)

(*c*) Cs 7 Å manganate ($a=5.103$ Å, $b=2.844$ Å, $c=7.406$ Å, $\beta=101.06°$)

Line No.	Intensity I/I_o (×100)	$d_{(meas.)}$ Å	$d_{(calc.)}$ Å	*hkl*	$d_{(meas.)}-d_{(calc.)}$ (×1000)
1	100	7.277	7.268	001	9
*2	26	3.634	3.634	002	0
3	1	2.514	2.521	$\bar{2}01$	–7
			2.504	200	10
* 4	1	2.473	2.473	110	0
5	1	2.412	2.412	$\bar{1}11$	0
6	1	2.243	2.239	201	4
*7	1	2.141	2.141	$\bar{1}12$	0
8	<1	1.957	1.960	112	–3
9	<1	1.891	1.899	202	–8
10	1	1.816	1.819	$\bar{1}13$	–3
			1.817	004	–1
11	<1	1.525	1.535	$\bar{1}14$	–10
12	1	1.469	1.459	$\bar{3}11$	10
13	<1	1.443	1.439	310	4
*14	1	1.422	1.422	020	0
			1.421	$\bar{3}12$	1
15	1	1.397	1.402	114	–5
			1.396	021	1
16	<1	1.370	1.370	311	0

TABLE 3. (*contd.*)

(*d*) Be 7 Å manganate ($a=4.915$ Å, $b=2.838$ Å, $c=7.338$ Å, $\beta=101.11°$)

Line No.	Intensity I/I_o (×100)	$d_{(meas.)}$ Å	$d_{(calc.)}$ Å	*hkl*	$d_{(meas.)}-d_{(calc.)}$ (×1000)
1	100	7.209	7.200	001	9
*2	14	3.600	3.600	002	0
*3	4	2.446	2.446	110	0
			2.432	$\bar{2}01$	14
4	2	2.397	2.411	200	–14
			2.400	003	–3
			2.388	$\bar{1}11$	9
*5	3	2.250	2.250	111	0
6	1	1.937	1.937	112	0
7	1	1.799	1.804	$\bar{1}13$	–5
			1.800	004	0
8	1	1.638	1.635	113	3
*9	3	1.419	1.419	020	0
10	1	1.402	1.399	310	3
11	1	1.394	1.392	021	2
			1.387	114	7

TABLE 3. (*contd.*)

(*e*) Sr 7 Å manganate ($a=5.123$ Å, $b=2.834$ Å, $c=7.129$ Å, $\beta=100.56°$)

Line No.	Intensity I/I_o (×100)	$d_{(meas.)}$ Å	$d_{(calc.)}$ Å	*hkl*	$d_{(meas.)}-d_{(calc.)}$ (×1000)	
1	3	7.599	7.544	⅔00	45	1)
2	100	7.009	7.008	001	1	
* 3	26	3.504	3.504	002	0	
4	2	2.539	2.521	$\bar{2}01$	18	
			2.518	200	21	
* 5	3	2.470	2.470	110	0	
6	3	2.400	2.398	$\bar{1}11$	2	
7	1	2.326	2.336	003	−10	
8	1	2.191	2.266	111	−75	
			2.243	201	−52	
9	2	2.114	2.110	$\bar{1}12$	4	
10	<1	1.922	1.938	112	−16	
11	1	1.778	1.779	$\bar{1}13$	−1	
12	1	1.759	1.752	004	7	
*13	2	1.461	1.461	$\bar{3}11$	0	
			1.444	310	17	
14	1	1.420	1.417	020	3	
			1.416	$\bar{3}12$	4	
*15	1	1.389	1.389	021	0	

1): This weak line, d (⅔ 0 0), was also observed in the electron diffraction (Fig. 4*d*).

TABLE 3. (*contd.*)

(*f*) Ba 7 Å manganate ($a=5.149$ Å, $b=2.834$ Å, $c=7.184$ Å, $\beta=101.42°$)

Line No.	Intensity I/I_o (×100)	$d_{(meas.)}$ Å	$d_{(calc.)}$ Å	*hkl*	$d_{(meas.)}-d_{(calc.)}$ (×1000)	
1	4	7.634	7.572	⅔00	62	1)
2	100	7.040	7.042	001	−2	
* 3	43	3.521	3.521	002	0	
4	2	2.541	2.541	$\bar{2}01$	0	
			2.524	200	17	
* 5	3	2.471	2.471	110	0	
6	3	2.406	2.406	$\bar{1}11$	0	
7	1	2.345	2.347	003	−2	
8	2	2.229	2.239	201	−10	
9	4	2.122	2.122	$\bar{1}12$	0	
10	1	1.932	1.936	112	−4	
11	1	1.873	1.882	202	−9	
12	2	1.792	1.791	$\bar{1}13$	1	
13	2	1.763	1.760	004	3	
14	1	1.621	1.625	113	−4	
15	<1	1.563	1.571	203	−8	
16	1	1.506	1.504	$\bar{1}14$	2	
*17	2	1.467	1.467	$\bar{3}11$	0	
18	1	1.444	1.447	310	−3	
19	1	1.428	1.427	$\bar{3}12$	1	
*20	1	1.417	1.417	020	0	
21	1	1.391	1.389	021	2	
22	<1	1.369	1.372	114	−3	
			1.371	311	−2	

1): This weak line, *d* (⅔ 0 0), was also observed in the electron diffraction (Fig. 4*e*).

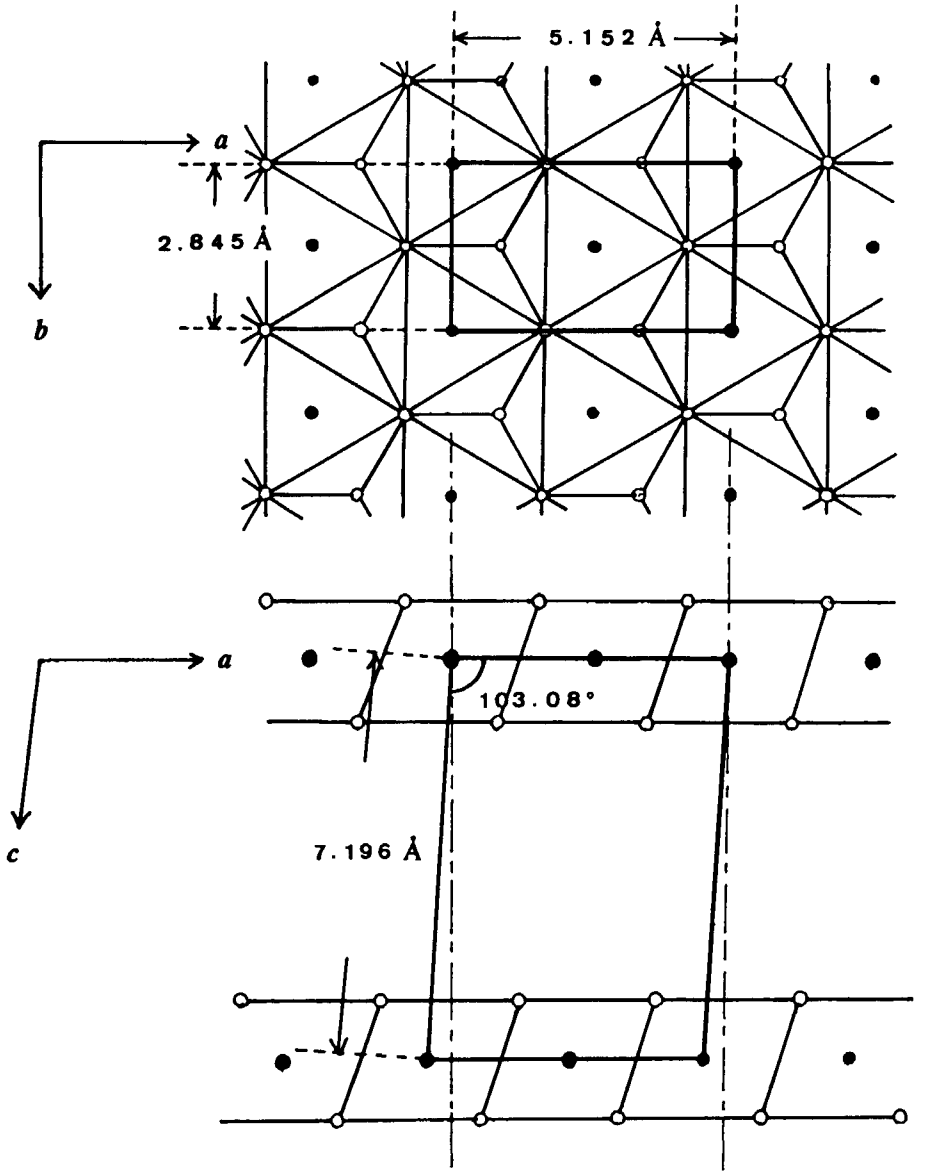

FIG. 5. Host manganese structure interpreted from the X-ray diffractograph of Li 7 Å manganate. The edge-shared [MnO_6] octahedral layer structure was interpreted from unit cell parameters of Li 7 Å manganate as a monoclinic crystal system.

cation position in the interlayer from the superlattice reflections in the *a–b* plane and streaking in the *a*-direction observed in electron diffractions.

Host manganate structure analysis. Fundamental hexagonal reflections in the *a–b* plane for the electron diffractions of synthetic manganates were interpreted as an isotropic manganate layer structure. However, the electron micrographs and the diffraction phenomena including superlattice reflections with orthorhombic system in the *a–b* plane and streaking in the *a*-direction, induced by substitution with

TABLE 4. Indexed interplanar spacings of Mg, Ca and Ni 10 Å manganates observed in X-ray diffraction lines on the basis of the indexed results for Li 7 Å manganate. The star marked lines (*) were chosen in order to match the indices of all lines as a monoclinic crystal system.

(*a*) Mg 10 Å manganate ($a=5.173$ Å, $b=2.834$ Å, $c=9.629$ Å, $\beta=93.97°$)

Line No.	Intensity I/I_o (×100)	$d_{(meas.)}$ Å	$d_{(calc.)}$ Å	hkl (×1000)	$d_{(meas.)}-d_{(calc.)}$
1	100	9.650	9.606	001	44
2	32	4.808	4.803	002	5
* 3	7	3.202	3.202	003	0
4	1	2.567	2.580	200	−13
* 5	2	2.536	2.536	$\bar{2}01$	0
* 6	2	2.484	2.484	110	0
			2.450	201	34
7	2	2.417	2.425	$\bar{1}11$	−8
			2.402	004	15
8	3	2.350	2.342	$\bar{2}02$	8
9	1	2.227	2.237	$\bar{1}12$	−10
10	<1	2.187	2.210	202	−23
11	1	2.097	2.081	$\bar{2}03$	16
12	<1	1.980	1.995	$\bar{1}13$	−15
13	<1	1.922	1.944	203	−22
			1.932	113	−10
			1.921	005	1
14	1	1.834	1.822	$\bar{2}04$	12
15	<1	1.744	1.756	$\bar{1}14$	−12
16	<1	1.679	1.700	204	−21
			1.699	114	−20
17	<1	1.604	1.601	006	3
18	1	1.469	1.471	310	−2
			1.467	$\bar{3}11$	2
19	< 1	1.446	1.441	311	5
			1.430	$\bar{3}12$	16
* 20	1	1.417	1.417	020	0
21	1	1.387	1.402	021	−15
			1.383	312	4

various cations, provide a useful insight into the anisotropic features and the actual three-dimensional structure of anionic host lattice.The most important electron diffraction characteristics are given in Table 5, indicating the superlattice indices in the [*h*00] and [0*k*0] directions, the folding number of the fundamental lattice along the *a*- and *b*-directions and the presence of streaking in the *a*-direction. Li, Mg, Ca, Sr, Ba and Ni manganates yield the different types of superlattice reflection patterns (Figs. 3 and 4). These patterns include a characteristic superlattice reflection, (⅔ 0 0), in the *a*-direction. The corresponding interplanar spacing is 7.4–7.9 Å. Chukhrov *et al.* (1979*a*) reported a new natural Ca-bearing birnessite, which is the structural analogue of synthetic Na-birnessite (Na manganate), in deep-sea micronodules from the selected area electron diffraction and spectrometer studies of energy dispersion of the nodules. The electron diffraction pattern in the *a*–*b* plane showed the orthorhombic superlattice reflections with a characteristic (⅔ 0 0) reflection, similar to those observed in this study (Figs. 3 and 4). For the manganates substituted by divalent cations, the larger the atomic number of substituent cation became, the stronger the intensity of reflection was observed. This result induces the appearance of a weak superlattice reflection line, (⅔ 0 0), adjacent to the *d*-value of 7 Å in the X-ray diffractions of Sr

TABLE 4. (*contd.*)

(*b*) Ca 10 Å manganate ($a=5.149$ Å, $b=2.828$ Å, $c=10.008$ Å, $\beta=93.96°$)

Line No.	Intensity I/I_o (×100)	$d_{(meas.)}$ Å	$d_{(calc.)}$ Å	*hkl*	$d_{(meas.)}-d_{(calc.)}$ (×1000)	
1	100	10.040	9.984	001	56	
2	<1	7.719	7.704	$\frac{2}{3}00$	15	1)
3	39	4.999	4.992	002	7	
* 4	11	3.328	3.328	003	0	
* 5	2	2.568	2.568	200	0	
6	<1	2.515	2.530	$\bar{2}01$	−15	
			2.496	004	19	
7	4	2.469	2.477	110	8	
8	4	2.448	2.447	201	1	
9	3	2.379	2.386	111	−7	
10	3	2.351	2.351	$\bar{2}02$	0	
*11	1	2.222	2.222	202	0	
12	1	2.171	2.190	112	−19	
13	1	2.114	2.105	$\bar{2}03$	9	
14	1	1.999	1.997	005	2	
15	1	1.971	1.969	203	9	
16	1	1.938	1.956	113	−18	
17	1	1.872	1.855	$\bar{2}04$	17	
18	1	1.720	1.731	204	−11	
			1.729	114	−9	
19	1	1.662	1.664	006	−2	
20	<1	1.637	1.632	$\bar{2}05$	5	
21	<1	1.523	1.526	205	−3	
22	2	1.468	1.465	310	3	
23	2	1.455	1.462	$\bar{3}11$	−7	
			1.437	311	18	
24	1	1.421	1.428	$\bar{3}12$	−7	
*25	1	1.414	1.414	020	0	
26	1	1.399	1.400	021	−1	

1): This weak line, *d* ($\frac{2}{3}$ 0 0), was also observed in the electron diffraction (Fig. 4*c*).

and Ba 7 Å and Ca and Ni 10 Å manganates (Table 3*e*, *f* and Fig. 1*b*, Table 4*b* and Fig. 2*a*, and Table 4*c* and Fig. 2*b*, respectively), resulting from the atomic scattering power of their cations. The extended X-ray absorption fine structure (EXAFS) measurements of synthetic 7 Å and 10 Å manganates revealed that the substituent cation position is above and below each vacancy in the edge-shared [MnO_6] octahedral layers (Crane, 1981; Stouff and Boulegue, 1988). In addition, the EXAFS measurements of oceanic hydrothermal Cu-rich 7 Å and 10 Å manganates revealed that the possible Cu position is also above and below the Mn vacancies (Stouff and Boulegue, 1989). Furthermore, Crane (1981) and Arrhenius and Tsai (1981) indicated that the essential vacancies in the manganate ion sheets in the most stable configuration are linearly arranged rather than hexagonally distributed over the sheet such as chalcophanite. The observed ($\frac{2}{3}$ 0 0) superlattice reflection also results from the linear distribution of the substituent cations, which are associated with the vacancies in the [MnO_6] layer, parallel to the *b*-axis in the interlayer. The distance between the cation rows parallel to the *b*-axis is seemingly three [MnO_6] octahedra wide. These above results suggest that the structures of synthetic 7 Å and 10 Å manganates are distinctly different from those of chalcophanite ($Zn_2Mn_6O_{14}\cdot 6H_2O$) and lithiophorite ($(Al,Li)MnO_2(OH)_2$), respectively, as one of the structural models for the phyllomanganates. The chalcophanite structure (Wadsley, 1955) consists of layers of edge-shared [MnO_6] octahedra and

TABLE 4. (*contd.*)

(*c*) Ni 10 Å manganate ($a=5.134$ Å, $b=2.849$ Å, $c=9.657$ Å, $\beta=\sim 90°$)

Line No.	Intensity I/I_o (×100)	$d_{(meas.)}$ Å	$d_{(calc.)}$ Å	*hkl*	$d_{(meas.)}-d_{(calc.)}$ (×1000)	
1	100	9.631	9.657	001	–26	
2	2	7.482	7.701	⅔00	–219	1)
3	45	4.823	4.829	002	–6	
* 4	8	3.219	3.219	003	0	
* 5	2	2.567	2.567	200	0	
6	5	2.485	2.491	110	–6	
			2.481	201	4	
7	4	2.400	2.414	004	–14	
			2.412	111	–12	
8	3	2.291	2.267	202	24	
9	4	2.205	2.214	112	–9	
10	1	2.028	2.007	203	21	
11	2	1.959	1.970	113	–11	
			1.931	005	28	
12	1	1.782	1.759	204	23	
13	2	1.733	1.734	114	– 1	
14	1	1.530	1.526	115	4	
*15	2	1.467	1.467	310	0	
16	1	1.450	1.450	311	0	
17	2	1.421	1.425	020	–4	
18	2	1.403	1.409	021	–6	
			1.403	312	0	
19	1	1.362	1.366	022	–4	
20	1	1.349	1.335	313	14	

1): This weak line, *d* (⅔00), was also observed in the electron diffraction (Fig. 4*f*).

single sheets of water molecules between which the Zn^{2+} ions are located. The stacking sequence along the *c*-axis is thus: -O-Mn-O-Zn-H_2O-Zn-O-Mn-O, and the perpendicular distance between consecutive [MnO_6] octahedral layers is about 7.16 Å. The water molecules are grouped in open double hexagonal rings, while vacancies exist in the layers of linked [MnO_6] octahedra, so that one out of every seven octahedral sites is unoccupied by manganese (Burns and Burns, 1979, 1981). The ordered vacancies in the chalcophanite structure are reflected in the hexagonal net of less intense reflections observed in electron diffraction patterns of platelets corresponding to the (001) plane (Chukhrov *et al.*, 1978, 1979*b*), which is evidently different from the orthorhombic superlattice reflections in the *a–b* plane and streaking in the *a*-direction observed in this study (Figs. 3 and 4). Lithiophorite also has a layer structure (Wadsley, 1952) in which layers of edge-shared [MnO_6] octahedra alternate with layers of [(Al,Li)$(OH)_6$] octahedra. The stacked sequence along the *c*-axis is: -O-Mn-O-OH-(Al,Li)-OH-O-Mn-O, and two consecutive [MnO_6] layers are about 9.5 Å apart. Vacancies do not occur in the sheets of linked [MnO_6] octahedra, nor in the [(Al,Li)$(OH)_6$], although vacancies may exist between the sheets (Burns and Burns, 1979, 1981). The X-ray and electron diffraction studies of a synthetic stoichiometric lithiophorite (Giovanoli *et al.*, 1973) have led to the hexagonal superlattice reflections in the *a–b* plane between [MnO_6] layers, probably indicating the long-range hexagonal distribution of Al and Li in the *a–b* plane different from the orthorhombic superlattice reflections in this study, and to the structural formula $[Mn_5^{4+}Mn^{2+}O_{12}]^{-}\cdot[Al_4Li_2(OH)_{12}]^{+}$ indicating the composition of the two layers stacked on each other. Giovanoli *et al.* (1973) concluded that lithiophorite has a fairly rigid lattice and that it differs fundamentally from the buserite group. The structure of natural asbolane, similar to that

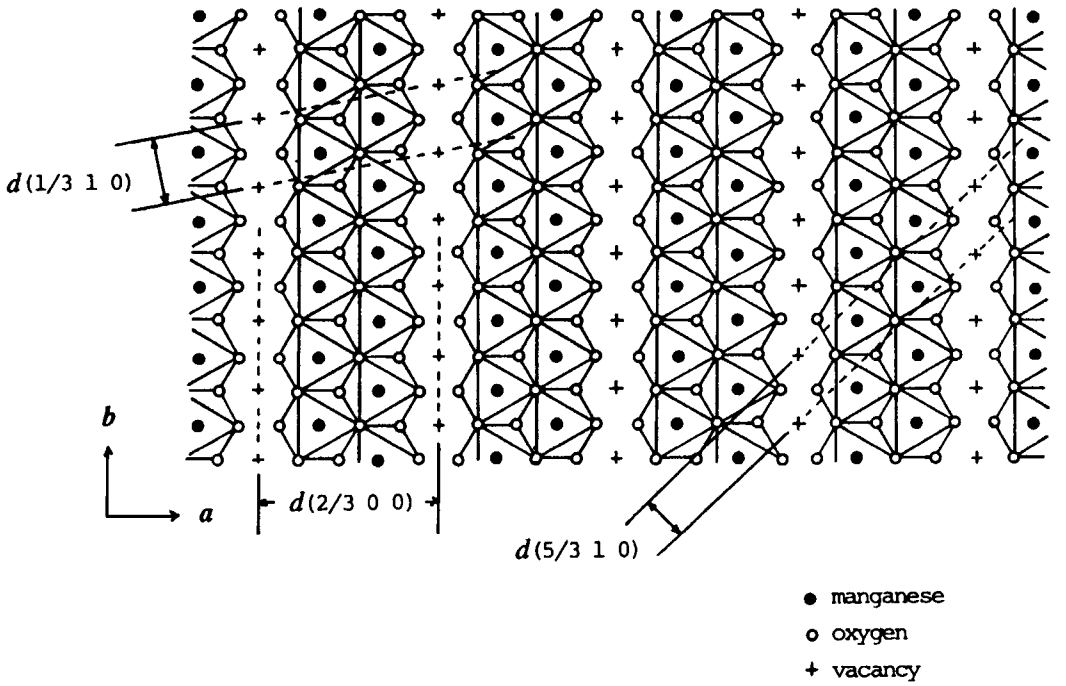

FIG. 6. The vacancy sites in the edge-shared [MnO_6] octahedral layer (*a*-*b*-plane) interpreted from the simple superlattice reflections in the electron diffractions for Mg and Ni manganates (Fig. 4*b* and *f*).

of lithiophorite, was also determined as a hybrid structure, in which layers of Mn^{4+} and Co–Ni octahedra alternate in the direction of the *c*-axis and form identically oriented hexagonal sublattices (Chukhrov *et al.*, 1980; Manceau *et al.*, 1987). This electron diffraction pattern showed two mixed hexagonal reflections in the *a*–*b* plane, evidently different from the orthorhombic superlattice reflections, associated with the fundamental hexagonal reflection as described above, in this study.

To interpret the cation position associated with the essential vacancies in the [MnO_6] octahedral layer, we chose the electron diffraction patterns of Mg and Ni manganates because of the higher exchange percentage 83–87%, of Mg^{2+} and Ni^{2+} to Na^{+} (Table 1) and same simple superlattice reflections, (⅔ 0 0), (⅓ 1 0), (⅔ 1 0) etc. (Fig. 4*b* and *f*). This simple superlattice reflections were also observed in the electron diffraction pattern of aged K/Na 7 Å manganate by Post and Veblen (1990). They also showed the fringes arising from the well-ordered 7.7 Å superstructure parallel to the *b*-axis in the K/Na manganate by high-resolution TEM image. This spacing is consistent with the interplanar spacing of (⅔ 0 0) found as a most important characteristic reflection in the electron diffraction patterns of Li, Mg, Ca, Sr, Ba and Ni manganates and in the X-ray diffraction lines of Sr and Ba 7 Å and Ca and Ni 10 Å manganate as described above. The superlattice reflections are seemingly interpreted that the vacancy sites in the [MnO_6] octahedral layer are linearly distributed parallel to the *b*-axis with three octahedra wide as shown in Fig. 6. However, from the molar ratio of divalent Mg and Ni to Mn (0.16–0.17 in Table 1) and the substituent cations position above and below each vacancy in the edge-shared [MnO_6] octahedral layers by the EXAFS measurements (Crane, 1981; Stouf and Boulegue, 1988, 1989), it was interpreted that one out of every six octahedral sites in the layer of linked [MnO_6] is vacant. Therefore, we will be able to propose one of the ideal configurations of Mg and Ni cations in the interlayer and essential vacancy sites in the [MnO_6] layers as shown in Fig. 7. This projection is in nearly good agreement with one of those for synthetic Na 7 Å manganate, $Na_4Mn_{14}O_{27}\cdot 9H_2O$, proposed by Giovanoli *et al.*, 1970*a* (Burns and Burns, 1977).

TABLE 5. Unit cell parameters estimated from X-ray diffraction data and superlattice planes interpreted from electron diffraction data

Sub. cation (charge)	Unit cell parameters				Superlattice reflection				Streaking
	a	*b*	*c*	β	[*h*00]	[0*k*0]	folding # of funda.		
	Å	Å	Å	°			*a*	*b*	
(+1)									
Li7 Å	5.152	2.845	7.196	103.08	(⅔ 0 0)	——	9	3	-
Na7 Å	5.164	2.848	7.314	102.96	N.D.	——	-	-	+ 1)
(Na7 Å	5.175	2.850	7.337	103.18	(Post and Veblen, 1990))				
Na* 10 Å	5.230	2.850	10.273	99.22	2)				
K7 Å	5.156	2.846	7.146	100.23	N.D. (0 ⅔ 0)		-	-	+ +1)
(K 7 Å	5.149	2.843	7.176	100.76	(Post and Veblen, 1990))				
Cs7 Å	5.103	2.844	7.406	101.06	ND. (0 ⅔ 0)		-	-	+ +1)
(+2)									
Be7 Å	4.915	2.838	7.338	101.11	——	——	1	1	- 3)
Mg*10 Å	5.173	2.834	9.629	93.97	(⅔ 0 0)	——	3	1	-
Mg 7 Å	4.940	2.842	6.863	95.26	2)				
(Mg 7 Å	5.049	2.845	7.051	96.65	(Post and Veblen, 1990))				
Ca*10 Å	5.149	2.828	10.008	93.96	(⅔ 0 0)	——	12	4	-
Sr7 Å	5.123	2.834	7.129	100.56	(⅔ 0 0)	(0 ½ 0)	12	4	-
Ba7 Å	5.149	2.834	7.184	101.42	(⅔ 0 0)	——	24	8	-
Ni*10 Å	5.134	2.849	9.657	~90	(⅔ 0 0)	——	3	1	-

[-: absence; +: weak; + +: strong]

*: 10 Å manganate for X-ray diffraction data, while collapsed to 7 Å spacing for electron diffraction data due to the exposure of the sample to high vacuum in the electron microscope.

1): N.D.: their superlattice indices could not be determined because of the observation of streaking (Fig. 3*c*, *d* and *e*).

2): Unit cell parameters determined from the X-ray diffraction data (data not shown) of Na 10 Å manganate (moist sample without drying) and of Mg 7 Å manganate (sample dried at 60°C for 1 day).

3): The electron diffraction of Be manganate showed only hexagonal fundamental reflections (Fig. 4*a*).

The folding number of the fundamental lattice to the superlattice reflections (Table 5) increases with the decrease in exchange percentage of substituent divalent cations to Na^+ (Table 1). This result probably indicates that the other cations, such as Li, Ca, Sr and Ba, in which characteristic superlattice reflections were observed, were also regularly distributed above and below vacancies according to the exchange percentage of cations to Na^+ on the basis of the essential vacancy sites (Fig. 7), which were interpreted from the simple superlattice reflections for Mg and Ni manganates. Therefore, the lowering of the exchange percentage of divalent cation to Na^+ possibly induces more complicate superlattice reflections (Fig. 4*c*, *d* and *e*) and larger folding number, resulting from the long-range order (Cullity, 1978; Beeston *et al.*, 1972). The actual unit cell parameters of synthetic 7 Å and 10 Å manganates must be determined from the location of substituent cation in the interlayer and are at least folding number (Table 5) times as large as the subcell. The actual superstructure for manganate probably has monoclinic or lower symmetry.

The streaking in the *a*-direction was observed in the electron diffractions for monovalent Na, K and Cs manganates (Fig. 3*c*, *d* and *e*) respectively). The streaking was intensified with the increase in ionic radius of substituent monovalent cation probably because of the degree of disordering of Na^+, K^+ and Cs^+ in the *a*-direction in the interlayer. This disordering of substituent cations also appears in the X-ray diffraction patterns of monovalent cation manganates as peak broadening (data not shown) and diffraction line disappearance (Table 2, Table 3*a*, *b* and *c*) with the increase in ionic radius of substituent cation,

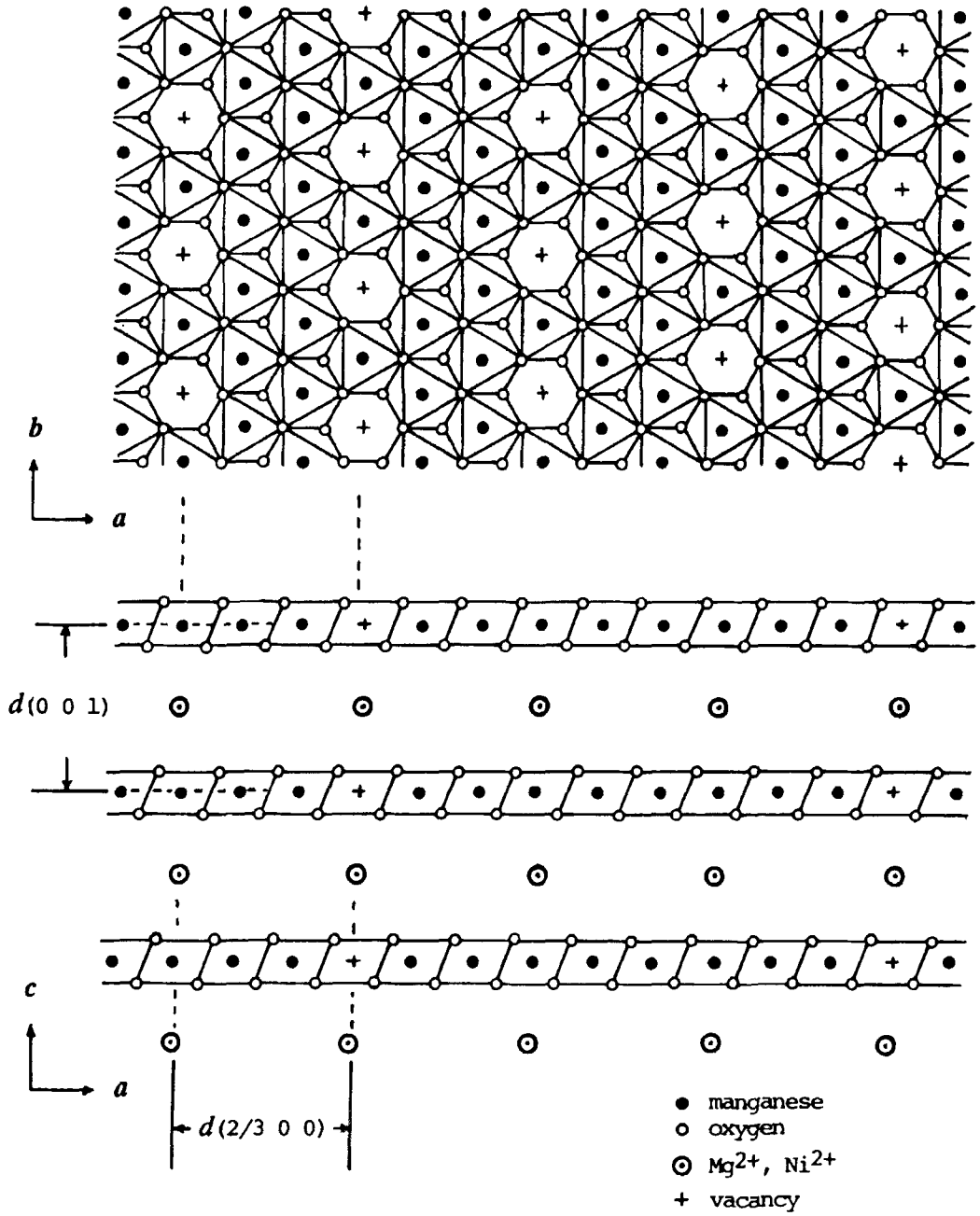

FIG. 7. The proposed synthetic manganate structure indicating the essential vacancy sites in the edge-shared [MnO_6] octahedral layer and possible cation position in the interlayer.

resulting from the structural disorder. Post and Veblen (1990) reported the observation of streaking in the *a*-direction in the electron diffraction patterns of Na and K 7 Å manganate, suggesting structural disorder. The (⅔ 0 0) diffraction line, which was observed in the X-ray

diffractions for the heavier divalent Sr and Ba 7 Å and Ca and Ni 10 Å manganates was not found in those for the monovalent cation manganates. This result also indicates the disordering of Na^+, K^+ and Cs^+ in the *a*-direction in the interlayer although their cations associate with essential vacancy sites regularly distributed in the layer of linked [MnO_6] octahedra as shown in Fig. 7. In addition to the streaking observed in the *a*-direction, the electron diffraction patterns of K and Cs manganates (Fig. 3*d* and *e*) include the same simple superlattice reflections, (0 ⅔ 0) and (1 ⅓ 0), probably due to several ordered arrangements of K^+ and Cs^+ in different interlayer regions in the same crystal as suggested by Post and Veblen (1990).

From the above results, the X-ray powder diffraction patterns for synthetic 7 Å and 10 Å manganates predominantly reveal only fundamental monoclinic structure of the edge-shared [MnO_6] octahedral layer. The subcells of all synthetic 7 Å and 10 Å manganates in this study have monoclinc unit cell parameters of which the angle β, *a* and *c* parameters change possibly with the type of substituent cation and the *b* parameter is relatively constant, in excellent agreement with those of Na, K and Mg 7 Å manganates reported by Post and Veblen (1990). However, the characteristic superlattice reflections in the electron diffraction patterns supply the information that several substituent cations are regularly distributed in the interlayer and occupy different positions depending upon the type of cation. The substituent cation position in the interlayer is attributed to essential vacancy sites regularly distributed in the layer of edge-shared [MnO_6] octahedra (Fig. 7), the exchange percentage of substituent cation to Na^+ and the ionic radius. In general, the electron and powder X-ray diffraction patterns of the synthetic birnessites and buserites are very similar to those of most natural samples, while the powder diffraction peaks for natural phases are more broadened, indicating a greater degree of structural disorder. The natural birnessites and buserites typically have more than one type of interlayer cation, which probably contributes to the structural disorder, and may have different numbers of interlayer cations than our synthetic phases.

Acknowledgements

We thank Prof. K. Matsunaga, Hokkaido University, for technical arrangements of the sample analysis by atomic absorption spectrophotometer.

References

Ahrens, L. H. (1952) The use of ionization potentials. Part 1. ionic radii of the elements. *Geochim. Cosmochim. Acta*, **2**, 155–69.

Arrhenius, G. and Tsai, A. G. (1981) Structure, phase transformation and prebiotic catalysis in marine manganate minerals. *Scripps Inst. Oceanogr. Ref. Ser.*, **81**, 1–19.

Arrhenius, G., Cheung, K. Crane, S., Fisk, M., Frazer, J., Korkisch, J., Mellin, T., Nakao, S., Tsai, A., and Wolf, G. (1979) Counterions in marine manganates. In *La Genèse des Nodules de Manganèse*, (C. Lalou, ed.), *Colloq. Int. C. N. R. S.*, **289**, 333–56.

Beeston, B. E. P., Horne, R. W. and Markham, R. (1972) *Electron diffraction and optical diffraction techniques.* In *Practical Methods in Electron Microscopy*, (A. M. Glauert, ed.), Vol. **1**, Part II, North-Holland/Elsevier, New York, 444 pp.

Burns, R. G. and Burns, V. M. (1977) The mineralogy and crystal chemistry of deep-sea manganese nodules, a polymetallic resource of the twenty-first century. *Phil. Trans. R. Soc. Lond. A.*, **286**, 283–301.

Burns, R. G. and Burns, V. M. (1979) Manganese oxides. In *Marine Minerals*, (R. G. Burns, ed.), Short Course Notes, Vol. **6**, Miner. Soc. Amer., Washington, D. C., pp. 1–46.

Burns, R. G. and Burns, V. M. (1981) Authigenic oxides. In *The Sea, VoL 7: The Oceanic Lithosphere*, (C. Emiliani, ed.), John Wiley, New York, pp. 875–914.

Burns, V. M. and Burns, R. G. (1978) Post-depositional metal enrichment processes inside manganese nodules from the north equatorial Pacific. *Earth Planet. Sci. Lett.*, **39**, 341–8.

Buser, W. and Graf, P. (1955*a*) Radiochemische Untersuchungen an Festkörpern, III. Ionen- und Isotopenaustauschreaktionen an Mangandioxyden und Manganiten. *Helv. Chim. Acta*, **38**, 810–29.

Buser, W. and Graf, P. (1955*b*) Differenzierung von Mangan (II) manganit und δ-MnO_2 durch Oberflächenmessung nach Brunauer-Emmett-Teller. *Helv. Chim. Acta*, **38**, 830–4.

Buser, W. and Grütter, A. (1956) Über die Nature der Manganknollen. *Schweiz Mineral Petrogr. Mitt.*, **36**, 49–62.

Chukhrov, F. V., Gorshkov, A. I., Rudnitskaya, E. S. and Sivtsov, A. V. (1978) The characteristics of birnessite. *Izvest. Akad. Nauk SSSR, ser. geol.*, no. **9**, 67–76.

Chukhrov, F. V., Gorshkov, A. I., Sivtsov, A. V. and Berezovskaya, V. V. (1979*a*) A new 14 Å mineral of the birnessite group in deep-sea micronodules. *Nature*, **280**, 136–7.

Chukhrov, F. V., Gorshkov, A. I., Sivtsov, A. V. and Berezovskaya, V. V. (1979*b*) New mineral phases of oceanic manganese microconcretions. *Izvest. Akad. Nauk SSSR,, ser. geol.*, no. **1**, 83–90.

Chukhrov, F. V., Gorshkov, A. I., Vitovskaya, I. V., Drits, V. A., Sivtsov, A. I. and Rudnitskaya, Ye. S. (1980) Crystallochemical nature of Co-Ni asbolan. *AN SSSR Izvestiya, ser. geol.*, no. **6**, 73–81. (Trans. *Internat. Geol. Rev.*, **24**, 598–604 (1982)).

Corliss, J. B., Lyle, M., Dymond, J. and Crane, K. (1978) The chemistry of hydrothermal mounds near the Galapagos rift. *Earth Planet. Sci. Lett.*, **40**, 12–24.

Crane, S. E. (1981) *Structural chemistry of the marine manganate minerals.* Ph.D. thesis (unpubl.), University of California, San Diego, 296 pp.

Cronan, D. S., Glasby, G. P., Moorby, S. A., Thomson, J., Knedler, K. E. and McDougall, J. C. (1982) A submarine hydrothermal manganese deposit from the south-west Pacific island arc. *Nature*, **298**, 456–8.

Cullity, B. D. (1978) *Elements of X-ray diffraction*, 2nd ed., Addison-Wesley, 555 pp.

Feitknecht, W. and Marti, W. (1945) Über die Oxydation von Mangan(II) hydroxid mit molekularem Sauerstoff. *Helv. Chim. Acta*, **28**, 129–56.

Giovanoli, R. (1980) On natural and synthetic manganese nodules. In *Geology and Geochemistry of Manganese*, (I. M. Varentsov and Gy. Grasselly, eds.), Akad. Kiado, Budapest, Vol. **1**, pp. 159–202.

Giovanoli, R. and Brütsch, R. (1979) Über die Oxidhydroxide des Mn(IV) mit Schichtengitter. 5 Mitteilung: Stöchiometrie, Austauschverhalten und die Rolle bei der Bindung von Tiefsee-Mangankonkretionen. *Chimia*, **33**, 372–6.

Giovanoli, R. and Bürki, P. (1975) Comparison of x-ray evidence of marine manganese nodules and non-marine manganese ore deposits. *Chimia*, **29**, 266–9.

Giovanoli, R., Stahli, E. and Feitknecht, W. (1970*a*) Über Oxidhydroxide des vierwertigen Mangans mit Schichtengitter. 1. Natrium-mangan (II,III) manganat (IV). *Helv. Chim. Acta*, **53**, 209–20.

Giovanoli, R., Stahli, E. and Feitknecht, W. (1970*b*) Über Oxihydroxide des vierwertigen Mangans mit Schichtengitter. 2. Mangan (II)-Manganat (IV). *Helv. Chim. Acta*, **53**, 453–64.

Giovanoli, R., Bühler, H. and Sokolowska, K. (1973) Synthetic lithiophorite: electron microscopy and x-ray diffraction. *J. Microsc.*, **18**, 271–84.

Giovanoli, R., Bürki, P., Giuffredi, S. and Stumm, W. (1975) Layer structured manganese oxide hydroxides. IV: The buserite group; structure stabilization of transition elements. *Chimia*, **29**, 517–20.

Glasby, G. P. (1972) The mineralogy of manganese nodules from a range of marine environments. *Mar. Geol.*, **13**, 57–72.

Hariya, Y. (1980) On the geochemistry and formation of manganese dioxide deposits. In *Geology and Geochemistry of Manganese* (I. M. Varentsov and Gy. Grasselly, eds.), Akad. Kiado, Budapest, Vol. **1**, pp. 353–66.

Manceau, A., Llorca, S. and Calas, G. (1987) Crystal chemistry of cobalt and nickel in lithiophorite and asbolane from New Caledonia. *Geochim. Cosmochim. Acta*, **51**, 105–13.

McKenzie, R. M. (1971) The synthesis of birnessite, cryptomelane, and some other oxides and hydroxides of manganese. *Mineral. Mag.*, **28**, 493–503.

Mellin, T. (1981) *Structural chemistry of synthetic manganate and iron compounds: implication for geochemistry of marine ferromanganese deposits.* Ph.D. thesis (unpubl.), University of Göteborg, Göteborg, 237 pp.

Moore, W. S. and Vogt, P. R. (1976) Hydrothermal manganese crusts from two sites near the Galapagos spreading axis. *Earth Planet. Sci. Lett.*, **29**, 349–56.

Post, J. E. and Veblen, D. R. (1990) Crystal structure determinations of synthetic sodium, magnesium, and potassium birnessite using TEM and the Rietveld method. *Amer. Mineral.*, **75**, 477–89.

Potter, R. M. and Rossman, G. R. (1979) The tetravalent manganese oxides: identification, hydration, and structural relationships by infrared spectroscopy. *Amer. Mineral.*, **64**, 1199–218.

Rosseinsky, D. R. (1965) Electrode potentials and hydration theories and correlations. *Chem. Rev.*, **65**, 467–90.

Shannon, R. D. and Prewitt, C. T. (1969) Effective ionic radii in oxides and fluorides. *Acta. Crystallogr.*, **B25**, 925–46.

Stouff, P. and Boulegue, J. (1988) Synthetic 10-A and 7-A phyllomanganates: their structures as determined by EXAFS. *Amer. Mineral.*, **73**, 1162–9.

Stouff, P. and Boulegue, J. (1989) Geochemistry and crystallochemistry of oceanic hydrothermal manganese oxyhydroxides showing Mn-Cu association. *Geochim. Cosmochim. Acta*, **53**, 833–43.

Tejedor-Tejedor, M. I. and Paterson, E. (1978) Reversibility of lattice collapse in synthetic buserite. *Int. Clay Conf.*, **27**, 501–8.

Turner, S., Siegel, M. D. and Buseck, P. R. (1982) Structural features of todorokite intergrowths in manganese nodules. *Nature*, **296**, 841–3.

Usui, A. (1979) *Mineralogical study of marine manganese nodules, synthesis of hydrous manganese oxides, and their implication to the genesis and geochemistry.* Ph.D. thesis (unpubl.), University of Tokyo, Tokyo, 175 pp.

Usui, A. and Nishimura, A. (1992) Submersible

observations of hydrothermal manganese deposits on the Kaikata seamount, Izu-Ogasawara (Bonin) arc. *Mar. Geol.*, **106**, 203–16.

Usui, A., Takenouchi, S. and Shoji, T. (1978) Mineralogy of deep sea manganese nodules and synthesis of manganese oxides: implication to genesis and geochemistry. *Mining Geol.*, **28**, 405–20. (In Japanese with English abstr.).

Usui, A., Melline, T. A., Nohara, M. and Yuasa, M. (1989) Structural stability of marine 10 Å manganates from the Ogasawara (Bonin) Arc: Implication for low-temperature hydrothermal activity. *Mar. Geol.*, **86**, 41–56.

Visser, J. W. (1969) A fully automatic program for finding the unit cell from powder data. *Appl. Cryst.*, **2**, 89–95.

Wadsley, A. D. (1950*a*) A hydrous manganese oxide with exchange properties. *J. Amer. Chem. Soc.*, **72**, 1782–4.

Wadsley, A. D. (1950*b*) Synthesis of some hydrated manganese minerals. *Amer. Mineral.*, **35**, 485–99.

Wadsley, A. D. (1952) The structure of lithiophorite, $(Al,Li)MnO_2(OH)_2$. *Acta Crystallogr.*, **5**, 676–80.

Wadsley, A. D. (1955) The crystal structure of chalcophanite, $ZnMn_3O_7.3H_2O$. *Acta Crystallogr.*, **8**, 165–72.

[*Manuscript received 13 September 1993: revised 1 November 1993*]